



Level distributions, partition functions, and rates of chirality changing processes for the torsional mode around O–O bonds

Ana C. Bitencourt, Mirco Ragni, Glauciete S. Maciel, Vincenzo Aquilanti, and Frederico V. Prudente

Citation: *J. Chem. Phys.* **129**, 154316 (2008); doi: 10.1063/1.2992554

View online: <http://dx.doi.org/10.1063/1.2992554>

View Table of Contents: <http://jcp.aip.org/resource/1/JCPSA6/v129/i15>

Published by the [American Institute of Physics](http://www.aip.org).

Additional information on *J. Chem. Phys.*

Journal Homepage: <http://jcp.aip.org/>

Journal Information: http://jcp.aip.org/about/about_the_journal

Top downloads: http://jcp.aip.org/features/most_downloaded

Information for Authors: <http://jcp.aip.org/authors>

ADVERTISEMENT

The advertisement banner features a green and yellow abstract background with flowing lines. The text 'AIPAdvances' is in a green font with a series of orange dots above it. Below this, the text 'Special Topic Section: PHYSICS OF CANCER' is written in white on a dark green background. At the bottom, the text 'Why cancer? Why physics?' is in yellow, and a blue button with white text says 'View Articles Now'.

Level distributions, partition functions, and rates of chirality changing processes for the torsional mode around O–O bonds

Ana C. P. Bitencourt,^{1,a)} Mirco Ragni,¹ Glauciete S. Maciel,¹ Vincenzo Aquilanti,¹ and Frederico V. Prudente²

¹*Dipartimento di Chimica, Università di Perugia, 06123 Perugia, Italy*

²*Instituto de Física, Universidade Federal da Bahia, 40210-340 Salvador, Bahia, Brazil*

(Received 23 June 2008; accepted 9 September 2008; published online 21 October 2008)

In view of the particular attention recently devoted to hindered rotations, we have tested reduced kinetic energy operators to study the torsional mode around the O–O bond for H₂O₂ and for a series of its derivatives (HOCl, HOOCN, HOOF, HOONO, HOOMe, HOOEt, MeOOMe, ClOOCl, FOCl, FOOF, and FOONO), for which we had previously determined potential energy profiles along the dihedral ROOR' angle [*R, R'* = H, F, Cl, CN, NO, Me (=CH₃), Et (=C₂H₅)]. We have calculated level distributions as a function of temperature and partition functions for all systems. Specifically, for the H₂O₂ system we have used two procedures for the reduction in the kinetic energy operator to that of a rigid-rotor-like one and the calculated partition functions are compared with previous work. Quantum partition functions are evaluated both by quantum level state sums and by simple classical approximations. A semiclassical approach, using a linear approximation of the classical path and a quadratic Feynman–Hibbs approximation of Feynman path integral, introduced in previous work and here applied to the torsional mode, is shown to greatly improve the classical approximations. Further improvement is obtained by the explicit introduction of the dependence of the moment of inertia from the torsional angle. These results permit one to discuss the characteristic time for chirality changes for the investigated molecules either by quantum mechanical tunneling (dominating at low temperatures) or by transition state theory (expected to provide an estimate of racemization rates in the high energy limit). © 2008 American Institute of Physics. [DOI: 10.1063/1.2992554]

I. INTRODUCTION

A systematic quantum chemical investigation of molecules containing the peroxidic bond has been reported recently.^{1–3} The emphasis was on the characterization of the torsional mode, which is responsible for the stereomutation, namely, the exchange between chiral enantiomers through the *trans* and *cis* barriers, a motivation being the understanding of the possible role of a collisional mechanism for such processes.⁴ We also estimated torsional levels and their populations as a function of temperature.

Interest on the specific features of torsional modes has been renovated recently: See, for example, Refs. 5–10 for spectroscopic investigations of separation of internal and rotational motions. With respect to the calculation of partition functions, of relevance both for thermodynamical and reaction kinetic problems, see Refs. 11–16 and references therein. In this paper we compute the partition functions according to well established recipes by explicit use of the calculated torsional levels and also give a test for simple classical and semiclassical approximations. In the calculation of the classical partition function we found it important to consider a correction proposed in Refs. 17 and 18 which uses features of the linear approximation of the classical path (LCP) approach and the quadratic Feynman–Hibbs (QFH) approximation of the Feynman path integral.

For H₂O₂, two schemes are considered for the calculations of the levels, and while overall agreement is found with a recent paper,¹⁴ advantages of using orthogonal vectors¹ and the explicit dependence of the effective moment of inertia on the dihedral angles are pointed out. Another important aspect of the calculation of the classical torsional partition function is the dependence of the moment of inertia on the geometrical parameters and of the dihedral angles. For discussions and calculations of the effective moment of inertia of molecules with internal rotation see, for example, Refs. 14 and 19 and references therein. In the present work we tested alternative expressions for the moment of inertia which can be considered as a constant only in a first approximation. However, a more general approach based on the kinetic energy operator takes into account the dependence from the dihedral angle. An additional case corresponds to the diatom-diatom approach using orthogonal vectors: In this case, the moment of inertia does not depend on the dihedral angle. We have verified that the explicit introduction of such a dependence on the dihedral angle improves the classical approximations for the torsional partition functions.

Furthermore, the results presented in this paper allow us to characterize the racemization rates, namely, for the process of stereomutation^{20,21} between the two enantiomeric forms connected by torsion around the O–O bond. Computed level splittings provide the time for quantum mechanical tunneling, which is the mechanism responsible for the chirality

^{a)}Electronic mail: carla@dyn.unipg.it.

TABLE I. Equilibrium geometries and *cis* and *trans* barriers calculated with the B3LYP//6-311++G(3df,3pd) method (Refs. 2 and 3). α_0 and α_1 are calculated using Eqs. (4) and (5). The bond lengths are expressed in angstrom, the angles in degree, and the barriers and α in cm^{-1} . In the case of the HOOH we have also used the diatom-diatom approach (Fig. 3) and $\hbar^2/2I_{\text{rot}}=40.412 \text{ cm}^{-1}$, $V_{\text{cis}}=2645.33 \text{ cm}^{-1}$, and $V_{\text{trans}}=396.81 \text{ cm}^{-1}$.

ROOR'	r_1	R_{OO}	r_2	θ_1	θ_2	φ	α_0	α_1	V_{cis}	V_{trans}
HOOH	0.966	1.447	0.966	100.8	100.8	112.5	40.150 8	0.658 787	2575.00	386.00
CIOOCl	1.748	1.362	1.748	111.5	111.5	84.8	2.258 21	1.102	3523.55	2174.54
FOOCl	1.497	1.281	1.802	108.0	112.9	86.1	2.671 24	1.162 58	6037.44	4713.87
FOOF	1.524	1.222	1.524	109.2	109.2	90.0	3.050 83	1.176 76	9717.72	8292.25
FOONO	1.494	1.308	1.662	106.9	107.0	88.6	2.470 51	0.881 361	4461.57	4575.85
HOOCi	0.970	1.410	1.730	102.4	110.1	88.8	21.264 6	0.950 122	2317.83	1618.94
HOOCN	0.970	1.475	1.290	99.6	108.5	111.9	21.337 1	0.806 641	1420.75	212.98
HOOF	0.973	1.359	1.467	103.8	106.2	84.9	21.777 8	0.909 959	3339.37	3545.44
HOONO	0.968	1.417	1.479	102.1	106.9	99.6	21.453 3	0.839 379	935.26	744.06
HOOMe	0.966	1.449	1.414	100.8	106.8	115.6	21.677 7	0.783 283	2080.00	151.92
HOOEt	0.966	1.451	1.424	100.4	107.6	114.5	21.334 9	0.797 795	2270.55	236.46
MeOOMe	1.410	1.460	1.410	105.2	105.2	180.0	3.071 79	0.722 354	3904.37	0.00

changing process at low temperatures, while for high temperatures the time of racemization is estimated by transition state theory using the computed partition functions.

The scheme of the paper is as follows. In the next section, we report the methodology regarding the torsional level calculations. Section III reports the quantum, classical, and semiclassical formulas used to evaluate the torsional partition functions. Section IV presents calculated results and discussions, in particular, regarding racemization times. The last section contains further remarks and some conclusions.

II. TORSIONAL LEVELS

In previous articles¹⁻³ we have presented a systematic study by quantum mechanical methods of a series of molecules, corresponding to substitutions of one or both hydrogens in hydrogen peroxide. First we have studied the effects of the substitution by one or two alkyl groups (CH_3OOH , $\text{C}_2\text{H}_5\text{OOH}$, and CH_3OOCH_3),² by halogen atoms (HOOF, HOOCi, ClOO, FOO, and ClOOCl), and by NO and CN.³ Data relevant to the present work are listed in Table I for the equilibrium *cis* and *trans* configurations. We have calculated the energy profiles along the torsional angle φ , ranging from

0° (the *cis* configuration) to 180° (the *trans* configuration) with a step of 1° optimizing the geometry at each angle. The resulting values are fitted to a cosine expansion

$$V(\varphi) = \sum_k C_k \cos(k\varphi), \quad (1)$$

where $k=0,1,2,\dots$. The coefficients C_k are obtained by a Newton–Raphson fitting to the calculated potential energy points and are given in Table II. An illustration of the distribution of levels obtained as described below is presented in Fig. 1 for the case of the HOOF molecule. References 1–3 provide further details.

A. Valence-type coordinates

The effective kinetic energy operator that we have employed for the calculation of energy levels is of the type used for example by Likar *et al.*²² for the HOOR systems. We have applied it for general ROOR' systems, where R and R' can be an atom or a group of atoms. Coordinates are described in Fig. 2. Then the kinetic energy operator can be written in the Hermitian (self-adjoint) form

TABLE II. Coefficients of $V(\varphi)$ (Fig. 2) of the expansion [Eq. (1)] in cm^{-1} .

Molecule	C_0	C_1	C_2	C_3	C_4	C_5	rms
HOOH ^a	835.52	1063.15	679.08	58.61	6.27	2.80	0.34
HOOH	830.01	1056.43	651.65	38.35	-1.50	0.76	0.36
CIOOCl	1622.33	417.49	1407.86	321.59	-185.75	-58.87	4.96
FOOCl	2995.76	268.38	2693.53	434.52	-307.62	-18.42	24.95
FOOF ^b	4908.90	268.92	4643.32	434.07	-457.64	61.29	61.17
FOONO	2302.31	-34.37	2294.01	-44.55	-45.47	22.19	26.56
HOOCi	1002.60	232.26	982.22	114.78	-18.82	2.56	0.66
HOOCN	460.28	583.97	360.79	19.95	-4.07	-0.01	0.16
HOOF	1761.99	-252.53	1708.83	145.40	-26.82	6.01	2.05
HOONO	466.30	170.23	407.18	-68.42	-32.13	-5.52	1.49
HOOMe	608.96	874.86	493.68	85.50	12.92	3.80	0.55
HOOEt	668.62	918.60	549.89	83.49	22.95	8.35	4.27
MeOOMe	1170.03	1737.84	753.23	192.16	19.27	22.50	7.19

^aThese coefficients refer to the expansion of the torsional energy profile $V(\Phi)$ as a function of the dihedral angle Φ (Fig. 3) of the orthogonal representation.

^bFor the FOOF system, we also have $C_6=-148.80 \text{ cm}^{-1}$ and $C_7=-41.99 \text{ cm}^{-1}$.

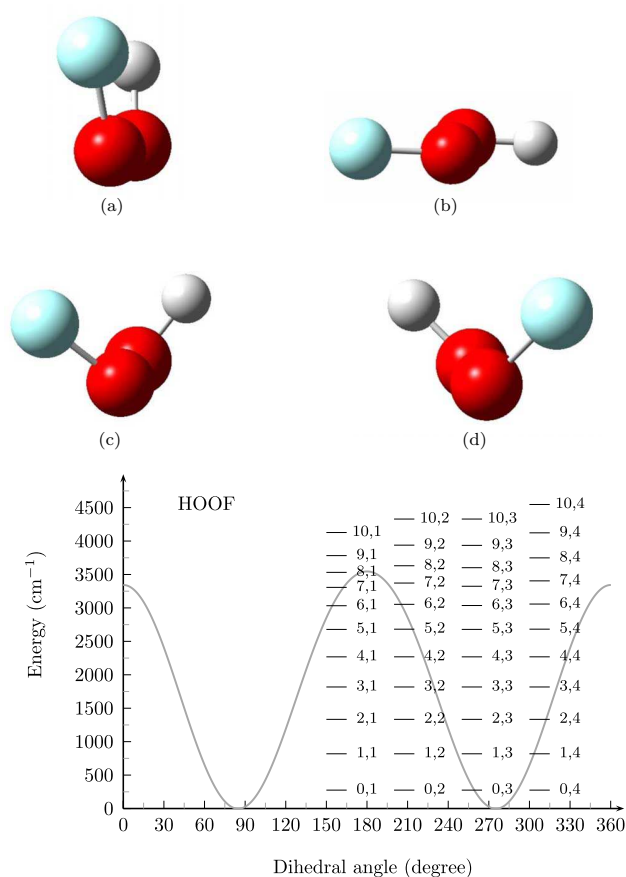


FIG. 1. (Color online) Illustration of the HOOF molecule in the (a) *cis* $\varphi=0^\circ$ and 360° , (b) *trans* $\varphi=180^\circ$, and both chiral equilibrium configurations (c) $\varphi=84.9^\circ$ and (d) $\varphi=275.1^\circ$. The figure also shows the torsional potential and the levels for the HOOF molecule [designated as $n\tau$ according to the nomenclature of the previous papers (Refs. 2 and 3)].

$$\hat{T}(\varphi) = -\frac{d}{d\varphi}\alpha(\varphi)\frac{d}{d\varphi} = -\frac{d}{d\varphi}\left(\frac{\hbar^2}{2I(\varphi)}\right)\frac{d}{d\varphi}, \quad (2)$$

with

$$\alpha(\varphi) = \alpha_0 + \alpha_1 \cos \varphi, \quad (3)$$

$$\alpha_0 = \frac{1}{\mu_{RO}r_1^2 \sin^2 \theta_1} + \frac{1}{\mu_{OR'}r_2^2 \sin^2 \theta_2} + \frac{1}{\mu_{OO}R_{OO}^2} \\ \times (\cot^2 \theta_1 + \cot^2 \theta_2) - \frac{2}{m_O R_{OO}} \left(\frac{\cot \theta_1}{r_1 \sin \theta_1} + \frac{\cot \theta_2}{r_2 \sin \theta_2} \right), \quad (4)$$

$$\alpha_1 = \frac{4 \cot \theta_1 \cot \theta_2}{m_O R_{OO}^2} - \frac{2}{m_O R_{OO}} \left[\frac{\cot \theta_2}{r_1 \sin \theta_1} + \frac{\cot \theta_1}{r_2 \sin \theta_2} \right], \quad (5)$$

where m_O is the oxygen mass and μ are reduced masses. All the geometrical parameters are assumed to have their equilibrium values as given in Fig. 2 and Table I. These equations are obtained using the Appendix of Ref. 22 and the work of Decius²³ (equation for $g_{\tau\tau}^4$ on p. 1028), who collaborated with Wilson, Jr. *et al.* in a book.²⁴ In the rigid-rotor-like

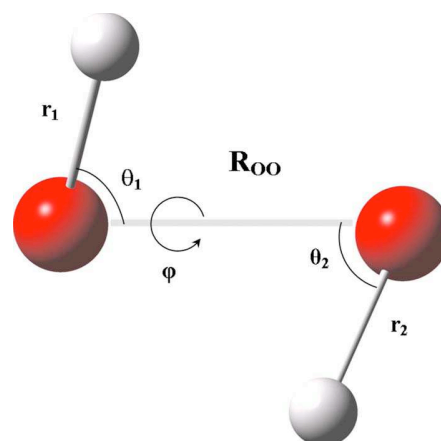


FIG. 2. (Color online) Illustration of the representations of the structure of the $ROOR'$ molecules in terms of the usual valence-type coordinates, where r_1 , R_{OO} , and r_2 are the interatomic distances, θ_1 and θ_2 are the bond angles, and φ is the dihedral angle.

kinetic operator (2) we have found it convenient to define an effective moment of inertia I as an explicit function of the torsional angle φ ,

$$I(\varphi) = \frac{\hbar^2}{2\alpha(\varphi)}. \quad (6)$$

The values of the α_0 and α_1 parameters are listed in Table I. These formulas are reasonable approximations provided that the variations in the other geometrical variables (bond lengths and bending angles) remain small as the dihedral angle varies. Therefore, for example, the cases of FOOF and CIOOF should be considered more closely regarding the role of R_{OO} variation (see Ref. 3). The choice of the equilibrium value for R_{OO} is appropriate for the low levels of relevance in this paper, but more accurate choices should be tested for the higher ones.

B. Orthogonal coordinates

For the H_2O_2 system we can alternatively exploit an orthogonal set of coordinates that well describe the torsional mode around the center of mass of the two fragments OH,^{1,25} so the kinetic part of the Hamiltonian presents only the second derivative of the angle Φ (Fig. 3) that describes this motion, scaled by a coefficient that depends of the masses of hydrogen and oxygen atoms, and of the molecular geometry at the equilibrium (see Table I and Ref. 1).

The torsional kinetic energy operator in orthogonal coordinates was given in a previous work,² where we also point out its advantages. It was obtained from the complete kinetic energy operator written in the diatom-diatom vector scheme [Eq. (23) of Ref. 25] and fixing all degrees of freedom except the dihedral angle Φ ; then

$$\hat{T}(\Phi) = -\frac{\hbar^2}{\mu_{OH}r_{OH}^2 \sin^2 \Theta} \frac{\partial^2}{\partial \Phi^2}, \quad (7)$$

where μ_{OH} is the reduced mass of the OH system and r_{OH} is the distance that separates the two atoms. Θ is the angle obtained connecting the center of mass of the first OH frag-

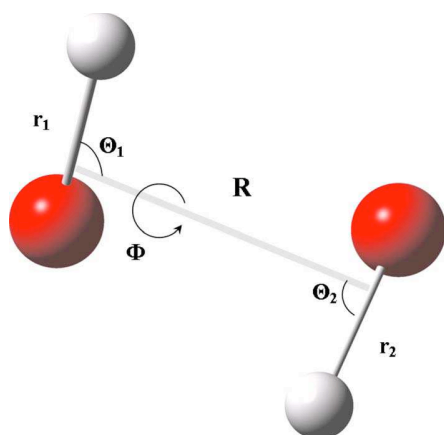


FIG. 3. (Color online) Illustration of the representations of the structure of the H_2O_2 molecule in terms of the orthogonal local coordinates or diatom-diatom vectors. r_1 and r_2 coincide with the OH bonds but R joins the centers of mass of the two OH groups.

ment to the other one and then pointing towards the second hydrogen; this angle is close but not identical to the angle $\hat{\text{H}}\hat{\text{O}}\hat{\text{O}}$, according to Fig. 3. Considering the moment of inertia of the diatom OH

$$I_{\text{OH}} = \mu_{\text{OH}} r_{\text{OH}}^2, \quad (8)$$

Eq. (7) can be written as

$$\hat{T} = -\frac{\hbar^2}{I_{\text{OH}} \sin^2 \Theta} \frac{\partial^2}{\partial \Phi^2} = -\frac{\hbar^2}{2I_{\text{ort}}} \frac{\partial^2}{\partial \Phi^2} \quad (9)$$

since

$$I_{\text{ort}} = \frac{1}{2} I_{\text{OH}} \sin^2 \Theta. \quad (10)$$

For H_2O_2 , for the coefficient in Eq. (9) we obtain $\hbar^2/2I_{\text{ort}} = 40.412 \text{ cm}^{-1}$, which is close to $\alpha_0 = 40.150 \text{ cm}^{-1}$ (and α_1 small, Table I), the value used for the valence coordinate reduced Hamiltonian. In Ref. 1 we also computed the torsional potential energy profile $V(\Phi)$ in orthogonal coordinates, which is conveniently expanded similarly to $V(\varphi)$ in Eq. (1), and the coefficients are listed in Table II (see also Ref. 2).

C. Symmetry classes

In view of the symmetry of the torsional potential by reflection with respect to φ or Φ equal to both 0 and π , corresponding to the two (*cis* and *trans*) planar configurations, the problem block diagonalizes in four symmetry classes (Floquet's theorem), denoted by the quantum label $\tau=1,2,3,4$. Levels within each symmetry classes are denoted by the quantum number $n=0,1,2,\dots$. Traditional basis sets in terms of sine and cosine functions were used, giving rise to secular equations, where the matrix elements are analytical integrals over trigonometric functions. So, for each quantum number n , there are the four well known Mathieu symmetries ($\tau=1,2,3,4$) and the wave functions are correspondingly expanded in orthonormal trigonometric basis sets (see, e.g., Ref. 26).

III. TORSIONAL PARTITION FUNCTION

A. Quantum formulas

The level distribution as a function of temperature has been calculated and already illustrated for some of the systems considered here in Ref. 2 and 3 using the formula

$$\frac{N_{n\tau}}{N} = \frac{e^{-\beta E_{n\tau}}}{\sum_{n'\tau'} e^{-\beta E_{n'\tau'}}}, \quad (11)$$

where $E_{n\tau}$ is the energy of the torsional state n and symmetry τ . As usual, $\beta=1/K_B T$, where K_B is Boltzmann's constant and T is the temperature.

The quantum mechanical torsional partition function $Q^q(T)$ can be evaluated at a given temperature from the energies of the levels^{12,27}

$$Q^q(T) = \sum_n \sum_{\tau=1,4} e^{-\beta E_{n\tau}}. \quad (12)$$

According to previous work (see, e.g., Ref. 14 and also Sec. V), only levels having symmetries $\tau=1$ and 4 (Ref. 26) are included.

B. Classical formulas

Several approximations for the torsional partition function for H_2O_2 have been discussed and tested in Ref. 14. In fact, when the temperature is sufficiently high, it is known that the quantum partition function can be usefully approximated by the classical expression^{14,28,29} (the T dependence is omitted from the notation for simplicity)

$$Q^c = \sqrt{\frac{I}{2\pi\beta\hbar^2}} \int_0^{2\pi/\sigma} e^{-\beta V(\varphi)} d\varphi, \quad (13)$$

where σ is an index number depending on the symmetric rotational group around the dihedral angle of the system, $\sigma=1$ in our cases. Equation (13) implies that the torsional moment of inertia (Sec. II) assumes a constant (effective or average) value.

Here we examine and assess some improvements that do not spoil the basic requirement of simplicity of implementation.

In general, I is related to the value of $\alpha(\varphi)$ according to Eq. (6). To calculate the moment of inertia from Eq. (6), as a first approximation we consider only the α_0 term, neglecting α_1 ; then

$$I = \frac{\hbar^2}{2\alpha_0} \quad (14)$$

and expression (13) can be written as

$$Q_{\alpha_0}^c = \sqrt{\frac{1}{4\pi\beta\alpha_0}} \int_0^{2\pi/\sigma} e^{-\beta V(\varphi)} d\varphi. \quad (15)$$

However, accounting for the dependence of I and α on φ leads to an improved approximation inserting the explicit functional dependence under the integral sign

$$Q_{\alpha}^c = \sqrt{\frac{1}{4\pi\beta}} \int_0^{2\pi/\sigma} \frac{e^{-\beta V(\varphi)}}{(\alpha_0 + \alpha_1 \cos \varphi)^{1/2}} d\varphi. \quad (16)$$

This expression provides a more general equation for the calculation of the classical partition function, which will be shown below to lead to more accurate results.

C. Semiclassical formulas

We have also calculated the partition function semiclassically using the formulation proposed in Refs. 17 and 18 (for a systematic discussion of alternatives, see Ref. 14). This method uses features of the LCP approach and the QFH approximation to the Feynman path integral. This LCP/QFH hybrid approach, which we denote by the superscript sc for “semiclassical,” consists in using in Eqs. (13), (15), and (16), instead of $V(\varphi)$, the following effective potential:

$$V(\varphi) \rightarrow V(\varphi) + \frac{\hbar^2\beta}{48I} \left[\frac{d^2}{d\varphi^2} V(\varphi) + \beta \left(\frac{d}{d\varphi} V(\varphi) \right)^2 \right], \quad (17)$$

where I is the moment of inertia. When I is calculated using only α_0 , Eq. (15), we have an approximation that we denote $Q_{\alpha_0}^{\text{sc}}$, while using Eq. (6), which accounts for the dihedral angle dependence, we have the approximation that we denote as Q_{α}^{sc} . In particular, for H_2O_2 , when I is calculated using Eq. (10), we have the approximation that we denote as $Q_{\text{ort}}^{\text{sc}}$.

IV. RESULTS AND DISCUSSION

To provide the torsional potential curves we have calculated the coefficients of expansion (1) for maximum k equal 6 for all systems (HOOH, HOOCI, HOOCN, HOOF, HOONO, HOOMe, HOOEt, MeOOMe, ClOOCl, FOOCI, and FOONO) except FOOF where k up to 8 was needed in order to minimize the root mean square (rms) deviation

$$\text{rms} = \sqrt{\frac{1}{N} \sum_{i=1}^N [V^0(\varphi_i) - V(\varphi_i)]^2}, \quad (18)$$

where V^0 is the potential energy calculated by quantum mechanical methods and V is the fitted potential at the dihedral angle φ_i . Data from Refs. 2 and 3 were used. The total number N was determined by the available grid points, which are spaced by 1° , in all cases, except for HOOH,^{2,3} where the spacing was 10° . The coefficients of expansion (1) are shown in Table II.

In the following we discuss the effects of the substituents on the potential energy profile along the torsional mode. The structural parameters and *cis* and *trans* barriers for all systems that we have considered are shown in Table I.

A. Hydrogen peroxide

In a previous article on H_2O_2 ,² we have presented the calculated torsional levels corresponding to both the geometrical (valence-type) and orthogonal (diatom-diatom) dihedral angles φ (Fig. 2) and Φ (Fig. 3), respectively. The results from the two procedures are similar. In particular, to study the statistical thermodynamics of torsional modes we have calculated their temperature distributions and the tor-

sional partition functions. Obviously in the orthogonal method, since there is a well defined expression for the moment of inertia, which is a constant as the torsional angle varies, the calculation is reliable also for the delocalized levels above the *trans* barriers. Table III shows the level distributions as a function of the temperature for the H_2O_2 system, evaluated by the orthogonal method (diatom-diatom approach).

In Table IV we list the torsional partition function at different temperatures for the H_2O_2 system. Q_{ort}^q and Q_{ort}^c are the quantum and classical partition functions using the diatom-diatom approach. Q_{ort}^q and Q^q are calculated using Eq. (12) directly from the levels of the symmetries $\tau=1$ and $\tau=4$ (see Sec. III A for this choice and also the remarks in Sec. V). Q_{ort}^c is calculated using Eqs. (10) and (13). For $Q_{\alpha_0}^c$ we use Eq. (15) and for Q_{α}^c we use Eq. (16). Finally $Q_{\alpha_0}^{\text{sc}}$ and Q_{α}^{sc} are calculated using the semiclassical or LCP/QFH approach described in Sec. III C. This approach turns out to be extremely accurate even at surprisingly low temperatures (see Table V and additional materials available from the authors).

B. Other systems

The features of the distribution of the torsional levels depend on the potential energy profile (*trans* and *cis* barriers) and of the masses of the atoms (moment of inertia).

Looking at the results for the other systems, one notes that the lowest levels, one for each of the four symmetries,²⁶ are nearly degenerate, $n=0$, $\tau=1, 2, 3, 4$, as shown in Figs. 1 and 4. This is particularly true when barriers (particularly the *trans*) are high and wide, so that tunneling is negligible, as in Fig. 1. Increasing n , this behavior persists under the lowest (*trans*) barrier, in proximity of which the degeneracy between the first two symmetries ($\tau=1$ and 2) and the other two ($\tau=3$ and 4) is removed; in systems such as HOOCN the two barriers are distant in energy and this effect is particularly visible, see levels (1,1), (1,2), (1,3), and (1,4), in Fig. 4. Going up with energy the levels encounter the higher (*cis*) barrier and here the effect on the symmetry is different. The energy of the first symmetry increases more slowly than the others, so that in the high energy limit it becomes degenerate with the fourth symmetry of the previous layer; at the same time, the levels with $\tau=2$ and 3 symmetries become degenerate. For energies close to the two barrier tops we notice an accumulation of states, typical of the nonharmonicity of the potentials.

Figure 1 exhibits the case of HOOF, where the *cis* and *trans* barriers are approximately of the same height and the behavior of the energy level sequence for the four symmetries is peculiar. Another limiting case is illustrated in Fig. 5, where the *trans* barrier is absent, but also applies when the *trans* barrier is so low that because of the masses involved no levels are supported under it. The methyl and the ethyl monosubstituted systems belong to this case.³ For the levels of these systems, degeneracy is appreciably removed even for the lowest levels.

In Table VI we report the partition functions at various temperatures for the HOOCI, HOOCN, HOOF, and HOONO

TABLE III. Distribution of the levels for the H₂O₂ system, evaluated with the orthogonal method (diatom-diatom approach).

Levels n, τ	Temperature (K)					
	100	200	300	600	1000	2400
0,1	0.266 777	0.231 775	0.200 983	0.142 830	0.104 713	0.057 944
0,2	0.266 777	0.231 775	0.200 983	0.142 830	0.104 713	0.057 944
0,3	0.225 771	0.213 220	0.190 108	0.138 912	0.102 980	0.057 542
0,4	0.225 771	0.213 220	0.190 108	0.138 912	0.102 980	0.057 542
1,1	0.006 264	0.035 516	0.057 553	0.076 431	0.071 957	0.049 558
1,2	0.006 264	0.035 516	0.057 553	0.076 431	0.071 957	0.049 558
1,3	0.001 124	0.015 047	0.032 464	0.057 404	0.060 600	0.046 136
1,4	0.001 124	0.015 047	0.032 464	0.057 404	0.060 600	0.046 136
2,1	0.000 061	0.003 500	0.012 278	0.035 302	0.045 268	0.040 855
2,2	0.000 061	0.003 500	0.012 278	0.035 302	0.045 268	0.040 855
2,3	0.000 003	0.000 765	0.004 455	0.021 265	0.033 397	0.035 993
2,4	0.000 003	0.000 765	0.004 455	0.021 264	0.033 396	0.035 993
3,1	0.000 000	0.000 147	0.001 481	0.012 260	0.024 000	0.031 363
3,2	0.000 000	0.000 147	0.001 481	0.012 259	0.023 998	0.031 363
3,3	0.000 000	0.000 026	0.000 469	0.006 902	0.017 002	0.027 167
3,4	0.000 000	0.000 026	0.000 469	0.006 899	0.016 998	0.027 164
4,1	0.000 000	0.000 004	0.000 145	0.003 831	0.011 943	0.023 449
4,2	0.000 000	0.000 004	0.000 144	0.003 824	0.011 930	0.023 439
4,3	0.000 000	0.000 001	0.000 044	0.002 123	0.008 380	0.020 231
4,4	0.000 000	0.000 001	0.000 044	0.002 106	0.008 341	0.020 192
5,1	0.000 000	0.000 000	0.000 014	0.001 195	0.005 937	0.017 525
5,2	0.000 000	0.000 000	0.000 013	0.001 160	0.005 831	0.017 394
5,3	0.000 000	0.000 000	0.000 005	0.000 705	0.004 327	0.015 361
5,4	0.000 000	0.000 000	0.000 004	0.000 639	0.004 079	0.014 988
6,1	0.000 000	0.000 000	0.000 002	0.000 447	0.003 290	0.013 703
6,2	0.000 000	0.000 000	0.000 001	0.000 350	0.002 842	0.012 894
6,3	0.000 000	0.000 000	0.000 001	0.000 289	0.002 534	0.012 291
6,4	0.000 000	0.000 000	0.000 000	0.000 188	0.001 954	0.011 029
7,1	0.000 000	0.000 000	0.000 000	0.000 174	0.001 869	0.010 828
7,2	0.000 000	0.000 000	0.000 000	0.000 097	0.001 312	0.009 342
7,3	0.000 000	0.000 000	0.000 000	0.000 094	0.001 294	0.009 290

systems. In Table VII there are the partition functions at various temperatures for the ClOOCl, FOCl, FOF, and FOONO molecules. In Table VIII we list the partition functions at various temperatures for the HOOMe, MeOOMe, and HOOEt systems. Q^g are calculated using Eq. (12) directly as before using the levels of symmetries $\tau=1$ and $\tau=4$ only. For $Q_{\alpha_0}^c$ we use Eq. (15) and for Q_{α}^c we use Eq. (16), obtaining a substantial improvement.

C. Intramolecular chirality changing rates

As an important application of the results of previous sections, Table IX shows the tunneling splittings and racem-

ization times for some of the investigated systems in the spirit of Fehrensen *et al.*²¹ The tunneling time is calculated directly from the level splitting of the symmetries $\tau=1$ and $\tau=4$ using the two level equation and the Heisenberg uncertainty principle,

$$\tau_0 \approx \frac{h}{2\Delta E}. \quad (19)$$

This can be interpreted as a racemization time at very low temperatures where only the ground state is populated. In the opposite limit of high temperatures the racemization time is modeled as occurring by passage over the *trans* barrier using

TABLE IV. Torsional partition functions at different temperature for the H₂O₂ system. Q_{ort}^g and Q_{ort}^c are the quantum and classical partition functions using the diatom-diatom approach. Q_{ort}^g and Q^g are calculated using Eq. (12) directly from the levels of the symmetries $\tau=1$ and $\tau=4$. Q_{ort}^c is calculated using Eqs. (10) and (13). $Q_{\alpha_0}^c$ uses Eq. (15) and Q_{α}^c uses Eq. (16). Q^{sc} is calculated using the LCP/QFH approach.

T (K)	Q_{ort}^g	Q_{ort}^c	$Q_{\text{ort}}^{\text{sc}}$	Q^g	$Q_{\alpha_0}^c$	Q_{α}^c	$Q_{\alpha_0}^{\text{sc}}$	Q_{α}^{sc}	Q^{g^a}	Q^{c^a}
200	0.613	0.769	0.606	0.624	0.775	0.778	0.614	0.617	0.644	0.796
300	1.075	1.183	1.072	1.089	1.191	1.196	1.081	1.086	1.116	1.220
600	2.306	2.351	2.301	2.319	2.359	2.368	2.310	2.319	2.358	2.406
1000	3.713	3.738	3.712	3.735	3.748	3.760	3.723	3.735	3.786	3.811
2400	7.770	7.776	7.770	7.815	7.805	7.821	7.799	7.815	7.892	7.897

^aReference 14.

TABLE V. Partition functions for H₂O₂ system at low temperatures evaluated using valence coordinates.

T (K)	Q^q	$Q_{\alpha_0}^c$	Q_{α}^c	$Q_{\alpha_0}^{sc}$	Q_{α}^{sc}
40	0.003	0.145	0.145	0.001	0.001
50	0.012	0.181	0.182	0.005	0.005
60	0.028	0.218	0.219	0.017	0.017
70	0.051	0.255	0.256	0.036	0.037
80	0.081	0.293	0.294	0.064	0.065
90	0.117	0.331	0.332	0.098	0.099
100	0.156	0.369	0.371	0.137	0.139
110	0.198	0.408	0.410	0.180	0.182
120	0.243	0.448	0.449	0.226	0.227
130	0.289	0.488	0.489	0.273	0.275
140	0.335	0.528	0.530	0.321	0.323
150	0.383	0.569	0.571	0.369	0.372
160	0.431	0.610	0.612	0.418	0.421
170	0.479	0.651	0.653	0.467	0.470
180	0.527	0.692	0.695	0.516	0.519
190	0.575	0.734	0.736	0.565	0.568

transition state theory with no tunneling correction²¹

$$\tau_T \approx \frac{h}{2k_B T} Q^q(T) \exp(E_{trans}/k_B T), \quad (20)$$

where E_{trans} is the *trans* barrier height (generally lower than the *cis* in the cases considered here, Table I), k_B the Boltzmann constant, and $Q^q(T)$ the partition function for the torsional mode, as given in Sec. III, Eq. (12).

V. FURTHER REMARKS AND CONCLUSIONS

In this work we exploited recently obtained torsional potential energy profiles for a series of ROOR' molecules to obtain torsional level distributions and partition functions as a function of temperature in order to provide a phenomenology of cases of qualitatively different profiles and barrier heights. Of the schemes investigated, the orthogonal set of coordinates is satisfactory for H₂O₂, but it is not obvious how to implement it in the general cases. Explicit consideration of the variation in the moment of inertia, suggested within the classical approximation, has been shown to extend

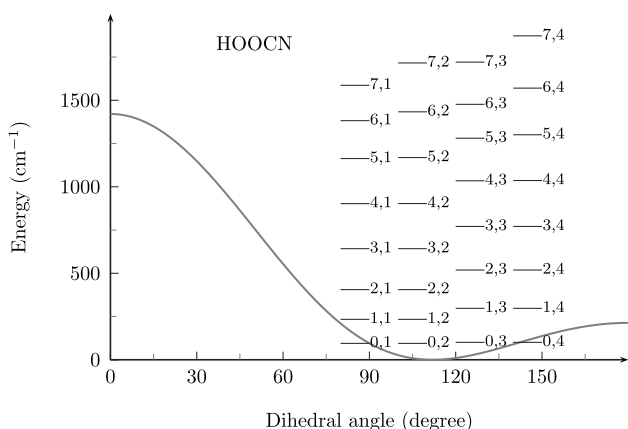


FIG. 4. Torsional energy profile as a function of the dihedral angle φ and energy levels n, τ for HOOCN.

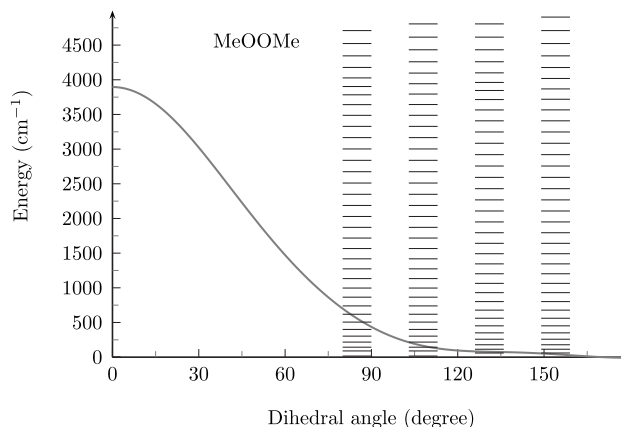


FIG. 5. Same as Fig. 4 for MeOOME (labels n, τ omitted).

the validity of the latter to lower temperatures. Further substantial improvement is obtained by the semiclassical approach of Sec. III C, denoted as LCP/QFH in Refs. 17 and 18.

An extensive investigation similar to this one but for the –S–S– bond, in the H₂S₂ and in a series of its derivatives, illustrates the trends of properties of interest here: Torsional barriers are in general higher than those encountered for the –O–O– bonds, with the specific consequence, for example, of lowering intramolecular racemization rates.

Additional remarks point out perspectives for future work. In the calculation of partition functions, we followed previous work (see, for example, Ref. 14), introducing only levels with symmetry quantum numbers $\tau=1$ and 4, consistently with the assumption that the total rotational angular

TABLE VI. Torsional partition functions at different temperatures for the HOOCI, HOOCN, HOOF, and HOONO. Q^q are calculated using Eq. (12) directly from the levels of the symmetries $\tau=1$ and $\tau=4$. $Q_{\alpha_0}^c$ uses Eq. (15) and Q_{α}^c uses Eq. (16). Q^{sc} is calculated using the LCP/QFH approach.

	T (K)	200	300	600	1000	2400
HOOCI	$Q_{\alpha_0}^c$	0.665	1.013	2.140	3.797	9.406
	Q_{α}^c	0.665	1.013	2.141	3.801	9.418
	$Q_{\alpha_0}^{sc}$	0.473	0.873	2.075	3.765	9.399
	Q_{α}^{sc}	0.473	0.873	2.076	3.769	9.411
	Q^q	0.480	0.877	2.077	3.769	9.411
HOOCN	$Q_{\alpha_0}^c$	1.463	2.180	4.097	6.329	12.362
	Q_{α}^c	1.476	2.199	4.128	6.366	12.401
	$Q_{\alpha_0}^{sc}$	1.374	2.124	4.075	6.319	12.360
	Q_{α}^{sc}	1.387	2.143	4.106	6.356	12.399
	Q^q	1.388	2.143	4.105	6.356	12.399
HOOF	$Q_{\alpha_0}^c$	0.506	0.757	1.536	2.646	6.967
	Q_{α}^c	0.505	0.756	1.533	2.642	6.960
	$Q_{\alpha_0}^{sc}$	0.277	0.575	1.437	2.591	6.952
	Q_{α}^{sc}	0.276	0.573	1.435	2.587	6.945
	Q^q	0.282	0.577	1.436	2.588	6.946
HOONO	$Q_{\alpha_0}^c$	0.977	1.531	3.358	5.712	12.032
	Q_{α}^c	0.980	1.536	3.367	5.724	12.046
	$Q_{\alpha_0}^{sc}$	0.836	1.443	3.328	5.700	12.030
	Q_{α}^{sc}	0.840	1.448	3.337	5.712	12.045
	Q^q	0.848	1.452	3.338	5.712	12.045

TABLE VII. Torsional partition functions at different temperatures for the ClOOCl, FOOC1, FOOF, and FOONO. Q^q are calculated using Eq. (12) directly from the levels of the symmetries $\tau=1$ and $\tau=4$. $Q_{\alpha_0}^c$ uses Eq. (15) and Q_{α}^c uses Eq. (16). Q^{sc} is calculated using the LCP/QFH approach.

	T (K)	200	300	600	1000	2400
ClOOCl	$Q_{\alpha_0}^c$	1.461	2.162	4.423	7.930	22.149
	Q_{α}^c	1.434	2.126	4.392	8.025	23.129
	$Q_{\alpha_0}^{\text{sc}}$	1.340	2.083	4.387	7.912	22.145
	Q_{α}^{sc}	1.311	2.045	4.356	8.007	23.124
	Q^q	1.312	2.046	4.356	8.007	23.124
FOOC1	$Q_{\alpha_0}^c$	1.313	1.776	3.236	5.295	13.790
	Q_{α}^c	1.295	1.752	3.198	5.249	13.919
	$Q_{\alpha_0}^{\text{sc}}$	1.102	1.642	3.176	5.262	13.780
	Q_{α}^{sc}	1.081	1.617	3.137	5.216	13.909
	Q^q	1.083	1.618	3.138	5.217	13.909
FOOF	$Q_{\alpha_0}^c$	1.114	1.490	2.658	4.241	10.040
	Q_{α}^c	1.109	1.484	2.648	4.228	10.051
	$Q_{\alpha_0}^{\text{sc}}$	0.865	1.327	2.581	4.197	10.024
	Q_{α}^{sc}	0.860	1.321	2.571	4.183	10.035
	Q^q	0.859	1.320	2.572	4.184	10.035
FOONO	$Q_{\alpha_0}^c$	1.678	2.301	4.253	6.999	17.839
	Q_{α}^c	1.685	2.311	4.274	7.040	18.036
	$Q_{\alpha_0}^{\text{sc}}$	1.518	2.201	4.209	6.975	17.832
	Q_{α}^{sc}	1.525	2.212	4.230	7.016	18.029
	Q^q	1.526	2.212	4.230	7.017	18.029

momentum contribution is separated out from the torsional mode. Interestingly, very recent attention has been devoted to the case of two coupled rigid rotors of different moments of inertia.^{6,30} The system considered in Ref. 6 is HOSH, and the problem is that of the torsion around the $-\text{O}-\text{S}-$ bond.

For the cases where the two moments of inertia are equal, conservation of both energy and angular momentum for a system viewed as involving either torsion plus external rotation or interaction of two rotors requires correlation of levels with symmetries $\tau=1$ and 4 with zero or even values

of the external rotation angular momentum quantum number K in units of \hbar (see Table I of Ref. 26). Conversely, levels with the two other symmetries, $\tau=2$ and 3, correlate with odd values. See also Ref. 10, where, however, reference to τ -labeled states is not explicitly made. As seen, for example, in Ref. 26 the four τ labels correlate with symmetries or antisymmetry wavefunctions with respect to either *trans* or *cis* barriers. In HOSH, the fact that the two rotors have different moments of inertia, see, e.g., Eq. (8), causes further level splitting for $\tau=2$ and 3 only. For the systems under

TABLE VIII. Torsional partition functions at different temperatures for the HOOMe, MeOOMe, and HOOEt. Q^q are calculated using Eq. (12) directly from the levels of the symmetries $\tau=1$ and $\tau=4$. $Q_{\alpha_0}^c$ uses Eq. (15) and Q_{α}^c uses Eq. (16). Q^{sc} is calculated using the LCP/QFH approach.

	T (K)	200	300	600	1000	2400
HOOMe	$Q_{\alpha_0}^c$	1.548	2.238	3.994	6.002	11.676
	Q_{α}^c	1.563	2.259	4.028	6.045	11.724
	$Q_{\alpha_0}^{\text{sc}}$	1.463	2.181	3.967	5.989	11.673
	Q_{α}^{sc}	1.478	2.203	4.001	6.031	11.721
	Q^q	1.476	2.201	4.000	6.030	11.721
HOOEt	$Q_{\alpha_0}^c$	1.362	2.024	3.764	5.770	11.465
	Q_{α}^c	1.375	2.043	3.796	5.812	11.516
	$Q_{\alpha_0}^{\text{sc}}$	1.261	1.959	3.735	5.755	11.462
	Q_{α}^{sc}	1.274	1.978	3.767	5.797	11.512
	Q^q	1.274	1.977	3.766	5.797	11.512
MeOOMe	$Q_{\alpha_0}^c$	3.512	5.019	8.855	13.225	26.244
	Q_{α}^c	3.893	5.529	9.645	14.261	27.678
	$Q_{\alpha_0}^{\text{sc}}$	3.492	5.003	8.845	13.219	26.242
	Q_{α}^{sc}	3.874	5.514	9.636	14.255	27.676
	Q^q	3.869	5.510	9.633	14.253	27.675

TABLE IX. Tunneling splittings and racemization times for some systems. ΔE and E_{trans} are in cm^{-1} .

System	E_{trans}	ΔE	τ_0 (s)	τ_T (s)			
				$T=200$ K	$T=300$ K	$T=600$ K	$T=2400$ K
HOOCN	212.98	5.81	1×10^{-12}	8×10^{-13}	5×10^{-13}	3×10^{-13}	1×10^{-13}
HOOH	396.81	11.60	3×10^{-12}	1×10^{-12}	6×10^{-13}	2×10^{-13}	1×10^{-13}
HOONO	744.06	0.04	6×10^{-10}	2×10^{-11}	4×10^{-12}	8×10^{-13}	2×10^{-13}
CIOOCl	2174.54	$<10^{-12}$	>7	1×10^{-6}	5×10^{-9}	3×10^{-11}	8×10^{-13}
HOOF	3545.44	4×10^{-7}	4×10^{-5}	4×10^{-3}	1×10^{-6}	3×10^{-10}	6×10^{-13}
FOONO	4575.85	$<10^{-11}$	>2	36.2	6×10^{-4}	1×10^{-8}	3×10^{-12}

focus in this paper, this issue would arise for cases such as HOOR or ROOR', but for them the removal of the energy degeneracy among levels under barriers is small, and moreover the influence on the partition functions calculated not including levels with $\tau=2$ and 3 becomes fully negligible. However, this may not be always the case and the full picture of separation of torsional modes in intramolecular dynamics still requires further investigation.

Besides the intramolecular chirality changing processes considered in this paper, alternative collisional mechanisms involve explicit consideration of intermolecular effects.³¹ Modeling of these latter phenomena so far rarely investigated in the literature requires classical, semiclassical, or quantum scattering calculations. See Ref. 32 for a study of the H_2O_2 –rare gas systems, a prototype of atom-flexible molecule interactions.

ACKNOWLEDGMENTS

We thank the Agenzia Spaziale Italiana (ASI) for support and the Italian Ministero per l'Università e la Ricerca (MIUR) for a PRIN grant. A.C.P.B. acknowledges a CAPES Brazilian fellowship. We thank D. G. Truhlar and S. L. Mielke for insightful correspondence and an anonymous referee for constructive criticism. F.V.P. thanks CNPq (Brazil) for financial support.

¹G. S. Maciel, A. C. P. Bitencourt, M. Ragni, and V. Aquilanti, *Chem. Phys. Lett.* **432**, 383 (2006).

²G. S. Maciel, A. C. P. Bitencourt, M. Ragni, and V. Aquilanti, *Int. J. Quantum Chem.* **107**, 2697 (2007).

³G. S. Maciel, A. C. P. Bitencourt, M. Ragni, and V. Aquilanti, *J. Phys. Chem. A* **111**, 12604 (2007).

⁴V. Aquilanti and G. S. Maciel, *Origins Life Evol. Biosphere* **36**, 435 (2006).

⁵G. Pelz, K. M. T. Yamada, and G. Winnewisser, *J. Mol. Spectrosc.* **159**, 507 (1993).

⁶K. M. T. Yamada, G. Winnewisser, and P. Jensen, *J. Mol. Struct.* **695**, 323 (2004).

⁷A. Bakasov, R. Berger, T.-K. Ha, and M. Quack, *Int. J. Quantum Chem.*

99, 393407 (2004).

⁸B. P. Winnewisser, M. Winnewisser, I. R. Medvedev, M. Behnke, F. C. De Lucia, S. C. Ross, and J. Koput, *Phys. Rev. Lett.* **95**, 243002 (2005).

⁹M. Winnewisser, B. P. Winnewisser, I. R. Medvedev, F. C. De Lucia, S. C. Ross, and L. M. Bates, *J. Mol. Struct.* **798**, 1 (2006).

¹⁰S. C. Ross and K. M. T. Yamada, *Phys. Chem. Chem. Phys.* **9**, 5809 (2007).

¹¹Y.-Y. Chuang and D. G. Truhlar, *J. Chem. Phys.* **112**, 1221 (2000); **121**, 7036 (2004); **124**, 179903 (2006).

¹²V. A. Lynch, S. L. Mielke, and D. G. Truhlar, *J. Chem. Phys.* **121**, 5148 (2004).

¹³V. A. Lynch, S. L. Mielke, and D. G. Truhlar, *J. Phys. Chem. A* **109**, 10092 (2005); **110**, 5965(E) (2006).

¹⁴B. A. Ellingson, V. A. Lynch, S. L. Mielke, and D. G. Truhlar, *J. Chem. Phys.* **125**, 084305 (2006).

¹⁵Y. K. Sturdy and D. C. Clary, *Phys. Chem. Chem. Phys.* **9**, 2065 (2007).

¹⁶Y. K. Sturdy and D. C. Clary, *Phys. Chem. Chem. Phys.* **9**, 2397 (2007).

¹⁷F. V. Prudente, A. Riganelli, and A. J. C. Varandas, *J. Phys. Chem. A* **105**, 5272 (2001).

¹⁸F. V. Prudente and A. J. C. Varandas, *J. Phys. Chem. A* **106**, 6193 (2002).

¹⁹K. S. Pitzer and W. D. Gwinn, *J. Chem. Phys.* **10**, 428 (1942).

²⁰M. Quack and M. Willeke, *J. Phys. Chem. A* **110**, 3338 (2006).

²¹B. Fehrens, D. Luckhaus, and M. Quack, *Chem. Phys.* **338**, 90 (2007).

²²M. D. Lika, J. E. Baggott, and F. F. Crim, *J. Chem. Phys.* **90**, 6266 (1989).

²³J. C. Decius, *J. Chem. Phys.* **16**, 1025 (1948).

²⁴E. B. Wilson Jr., J. C. Decius, and P. C. Cross, *Molecular Vibrations* (Dover, New York, 1980).

²⁵M. Ragni, A. C. P. Bitencourt, and V. Aquilanti, *Int. J. Quantum Chem.* **107**, 2870 (2007).

²⁶R. H. Hunt, R. A. Leacock, C. W. Peters, and K. T. Hecht, *J. Chem. Phys.* **42**, 1931 (1965).

²⁷A. Riganelli, F. V. Prudente, and A. J. C. Varandas, *Phys. Chem. Chem. Phys.* **18**, 4121 (2000).

²⁸A. Riganelli, F. V. Prudente, and A. J. C. Varandas, *J. Phys. Chem. A* **105**, 9518 (2001).

²⁹A. P. A. Urbano, F. V. Prudente, A. Riganelli, and A. J. C. Varandas, *Phys. Chem. Chem. Phys.* **3**, 5000 (2001).

³⁰J. T. Hougen, *Can. J. Phys.* **62**, 1392 (1984).

³¹V. Aquilanti, G. Grossi, A. Lombardi, G. S. Maciel, and F. Palazzetti, "The origin of chiral discrimination: Supersonic molecular beam experiments and molecular dynamics simulations of collisional mechanisms," *Phys. Scr.* (in press).

³²P. R. B. Barreto, A. F. A. Vilela, A. Lombardi, G. S. Maciel, F. Palazzetti, and V. Aquilanti, *J. Phys. Chem. A* **111**, 12754 (2007).